

Quantum magnetism of bosons with synthetic gauge fields in one-dimensional optical lattices: a Density Matrix Renormalization Group study

Marie Piraud¹, Zi Cai¹, Ian P. McCulloch², and Ulrich Schollwöck¹

¹ *Fakultät für Physik, LMU München, Theresienstrasse 37, D-80333 München, Germany*

² *Centre for Engineered Quantum Systems, School of Physical Sciences,
The University of Queensland, Brisbane, Queensland 4072, Australia*

(Dated: September 26, 2018)

In this paper, we provide a comprehensive study of the quantum magnetism in the Mott insulating phases of the 1D Bose-Hubbard model with abelian or non-abelian synthetic gauge fields, using the Density Matrix Renormalization Group (DMRG) method. We focus on the interplay between the synthetic gauge field and the asymmetry of the interactions, which give rise to a very general effective magnetic model: a XYZ model with various Dzyaloshinskii-Moriya (DM) interactions. The properties of the different quantum magnetic phases and phases transitions of this model are investigated.

PACS numbers: 67.85.Fg, 05.30.Rt, 75.10.Pq

I. INTRODUCTION

Recently, significant effort has been devoted to the realization of synthetic gauge fields for electrically neutral atoms [1–3]. By suitably coupling the atoms to laser fields, experimentalists have successfully created both abelian (effective magnetic fields [4, 5]) and non-abelian gauge potentials (effective spin-orbit coupling [6]) in ultracold atomic systems, where the neutral atoms subjected to synthetic gauge fields exhibit a variety of interesting phenomena, including the Hofstadter fractal spectrum [7–9], spin-orbit coupled Bose-Einstein condensates [6, 10–17], as well as spin-orbit coupled degenerate Fermi gases [18–20]. While most of these studies focus on the weakly interacting regime, the addition of a tunable optical lattice enables us to investigate the strongly correlated Mott insulating phases in the presence of gauge fields, where the interplay between strong interactions and synthetic gauge fields can give rise to exotic quantum magnetism that is difficult to access in solid state physics [21–30].

When the optical lattice is sufficiently deep to drive the system into the Mott insulating phase, the charge fluctuations are suppressed and the physics can be captured by an effective magnetic superexchange model. In the absence of a synthetic gauge field, it is well known that the effective Hamiltonian is described by an anisotropic Heisenberg model (XXZ model) [31, 32], where the anisotropy is determined by the asymmetry of the interactions in spin or quasi-spin space (the ratio between the inter-species and intra-species interaction strength). Introducing synthetic gauge fields into the Mott insulating phases, as we will show below, gives rise to a Dzyaloshinskii-Moriya (DM) interaction [33, 34], which is strongly reminiscent of its counterpart in strongly correlated electronic materials e.g. in the cuprate superconductor $\text{YBa}_2\text{Cu}_3\text{O}_6$ [35, 36] or in low-dimensional magnetic materials [37, 38]. In electronic materials, the spin-independent interaction (Coulomb interaction) causes the leading magnetic superexchange model to be

an isotropic Heisenberg model. It is known that for the 1D isotropic Heisenberg model, the additional DM interaction can be gauged away by performing a spin rotation [39]. However, for ultracold bosons with spin degrees of freedom, the situation is different: the inter-species and intra-species scattering lengths can be tuned within a broad range using Feshbach resonances [40, 41]. This leads to an asymmetry of the interactions as well as an anisotropy in the Heisenberg model – where the DM interaction can no longer be gauged away – and plays an important role in determining the magnetic properties of the system.

In this paper, we provide a comprehensive analysis of the quantum magnetism of the Mott insulating phases of the 1D Bose-Hubbard model with both abelian and non-abelian synthetic gauge fields using the Density Matrix Renormalization Group (DMRG) method [42, 43]. We show that the interplay between the synthetic gauge field and the asymmetry of the interactions gives rise to a XYZ model with different DM interactions (with DM vectors along the x, y , and z -directions), which is the most general form for a 1D spin-1/2 quantum magnetic model with two-site nearest-neighbor interactions. We explore the phase diagram of this model, and analyze the quantum phases and phase transitions that this model exhibits.

II. MODEL AND HAMILTONIAN

We consider an interacting two-component gas of bosons in a one-dimensional lattice, subject to a spin-dependent artificial magnetic field and a synthetic spin-orbit coupling of Rashba type, described by the Hamiltonian

$$\mathcal{H} = \mathcal{H}_t + \mathcal{H}_{\text{SOC}} + \mathcal{H}_U. \quad (1)$$

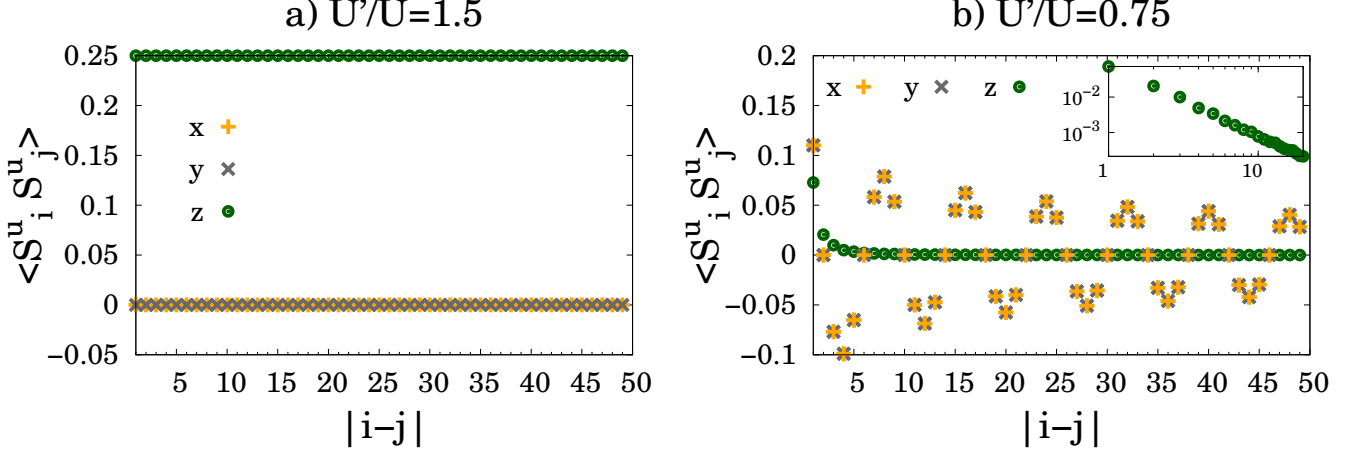


Figure 1: (Color online) Correlation functions in the ground state of Hamiltonian (5). Shown are $\langle S_i^x S_j^x \rangle$ (orange plus signs), $\langle S_i^y S_j^y \rangle$ (gray crosses) and $\langle S_i^z S_j^z \rangle$ (green dots) for $\beta = \pi/8$ and (a) $U'/U = 1.5$ and (b) $U'/U = 0.75$. The inset of (b) shows $\langle S_i^y S_j^y \rangle$ in log/log scale.

The kinetic part $\mathcal{H}_t + \mathcal{H}_{\text{SOC}}$ reads

$$\begin{aligned} \mathcal{H}_t &= -t \cos \alpha \sum_j \left[b_{j+1,\uparrow}^\dagger b_{j,\uparrow} e^{i\beta} + b_{j+1,\downarrow}^\dagger b_{j,\downarrow} e^{-i\beta} \right] + \text{h.c.} \\ \mathcal{H}_{\text{SOC}} &= -t \sin \alpha \sum_j \left[b_{j+1,\uparrow}^\dagger b_{j,\downarrow} - b_{j+1,\downarrow}^\dagger b_{j,\uparrow} \right] + \text{h.c.}, \quad (2) \end{aligned}$$

where t is the hopping amplitude, $b_{j,\uparrow/\downarrow}$ is the bosonic annihilation operator, j is the site index, and \uparrow, \downarrow denotes the two bosonic species ('spin' degree of freedom), β represents the strength of a spin-dependent magnetic field, where the different bosonic species feel opposite magnetic fields, and α denotes the strength of the 1D Rashba spin-orbit coupling, which allows spin-flipping tunneling. The interaction part of the Hamiltonian reads

$$\mathcal{H}_U = \frac{U}{2} \sum_{j\sigma} [n_{j,\sigma}(n_{j,\sigma} - 1)] + U' \sum_j n_{j,\uparrow} n_{j,\downarrow}, \quad (3)$$

where $\sigma = \uparrow, \downarrow$, and U (respectively U') represents the strength of the intra- (resp. inter-) species interaction.

When the interactions are strong enough to drive the system at unit filling into a Mott insulating phase, charge fluctuations are suppressed, and the physics is captured by an effective magnetic model. Using the spin-1/2 representation [31] $S_j^z = n_{j,\uparrow} - n_{j,\downarrow}$, $S_j^x = b_{j,\uparrow}^\dagger b_{j,\downarrow} + b_{j,\downarrow}^\dagger b_{j,\uparrow}$ and $S_j^y = -i(b_{j,\uparrow}^\dagger b_{j,\downarrow} - b_{j,\downarrow}^\dagger b_{j,\uparrow})$, the leading terms of the effective super-exchange Hamiltonian can be derived as:

$$\mathcal{H}_s = \sum_j \left[\sum_{u=x,y,z} J_u S_j^u S_{j+1}^u + \mathbf{D} \cdot (\mathbf{S}_j \times \mathbf{S}_{j+1}) \right]. \quad (4)$$

The Heisenberg terms are anisotropic in all three direc-

tions (XYZ model):

$$\begin{aligned} J_x &= J_0 [\sin^2 \alpha - \cos^2 \alpha \cos(2\beta)]; \\ J_y &= -J_0 [\sin^2 \alpha + \cos^2 \alpha \cos(2\beta)]; \\ J_z &= J_0 (-2U'/U + 1) [\cos^2 \alpha - \sin^2 \alpha], \end{aligned}$$

with $J_0 = 4t^2/U'$. The parameter U'/U characterizes the asymmetry of the interactions, and $U'/U = 1$ represents SU(2) symmetric interactions in spin space. The Dzyaloshinskii-Moriya (DM) interaction [33, 34] is characterized by a three-dimensional vector \mathbf{D} with:

$$\begin{aligned} D_x &= J_0 \frac{U'}{U} \sin(2\alpha) \sin \beta; \\ D_y &= J_0 \frac{U'}{U} \sin(2\alpha) \cos \beta; \\ D_z &= J_0 \cos^2 \alpha \sin(2\beta). \end{aligned}$$

Although there are only three independent parameters α , β and U'/U , the effective magnetic model given in Eq. (4) is one of the most general forms for a 1D spin-1/2 quantum magnetic model with two-site nearest-neighbor interactions.

III. BOSE-HUBBARD HAMILTONIAN WITH SPIN-DEPENDENT MAGNETIC FIELD

Let us first focus on a relatively simple case in which only an abelian synthetic gauge field is present (i.e. $\alpha = 0$). This case is directly relevant to current experiments with ultra-cold atoms [8, 9, 44]. If the different (spin) species experience the same magnetic field, the magnetic field has no effect on the superexchange magnetic Hamiltonian; we thus focus on the case in which spin- \uparrow and \downarrow bosons feel an equal and opposite magnetic

field. For $\alpha = 0$, Eq. (4) reduces to an anisotropic Heisenberg model (XXZ) with a DM interaction along the z -direction:

$$\mathcal{H}_s = J_0 \sum_j \left[-\cos(2\beta) (S_j^x S_{j+1}^x + S_j^y S_{j+1}^y) + \left(-2\frac{U'}{U} + 1 \right) S_j^z S_{j+1}^z + \sin(2\beta) (S_j^x S_{j+1}^y - S_j^y S_{j+1}^x) \right]. \quad (5)$$

Since the anisotropy of the Heisenberg model and the DM vector are along the same direction, the DM interaction can be gauged away by performing a rotation of the local spin basis for \mathbf{S}_j around the z -axis by an angle $2j\beta$: $S_j^x = \cos(2j\beta)S_j'^x + \sin(2j\beta)S_j'^y$, $S_j^y = \cos(2j\beta)S_j'^y - \sin(2j\beta)S_j'^x$ and $S_j^z = S_j'^z$, which leads to an XXZ model without DM interactions [45]

$$\mathcal{H}_s'' = J_0 \sum_j \left[- (S_j'^x S_{j+1}'^x + S_j'^y S_{j+1}'^y) + \left(1 - 2\frac{U'}{U} \right) S_j'^z S_{j+1}'^z \right]. \quad (6)$$

The phase diagram of this model has been thoroughly investigated [46, 47]. As a result, the ground state of Hamiltonian (5) will exhibit a gapped ferromagnetic (FM) state polarized in the z -direction for $U'/U > 1$. This is illustrated in Fig. 1(a), where we show the spin-spin correlation functions $\langle S_i^u S_j^u \rangle$ (with $u \in \{x, y, z\}$) in the ground state of Eq. (5) for $\beta = \pi/8$ and $U'/U = 1.5$. For $0 < U'/U < 1$ the ground state of Hamiltonian (5) is a gapless phase that follows from the XY phase of the XXZ model, with algebraically decaying correlations. However, due to the rotation from the mapping, the correlations in the x and y -directions exhibit spiral order, with a period of π/β sites. This is shown in Fig. 1(b) where the spin-spin correlations are plotted for $\beta = \pi/8$ and $U'/U = 0.75$: $\langle S_i^x S_j^x \rangle$ and $\langle S_i^y S_j^y \rangle$ oscillate with a period of 8 sites.

IV. BOSE-HUBBARD HAMILTONIAN WITH RASHBA SOC

We now study the case of a non-abelian synthetic gauge field. We consider the Rashba type of spin-orbit coupling in 1D, which has been implemented experimentally for atoms in the continuum [6, 11]. Proposals for schemes to implement it on lattices also exist [2, 48]. In the case $\beta = 0$, equation (4) simplifies to:

$$\mathcal{H}_s = J_0 \sum_j \left[-\cos(2\alpha) S_j^x S_{j+1}^x - S_j^y S_{j+1}^y + \left(-2\frac{U'}{U} + 1 \right) \cos(2\alpha) S_j^z S_{j+1}^z + \frac{U'}{U} \sin(2\alpha) (S_j^z S_{j+1}^x - S_j^x S_{j+1}^z) \right]. \quad (7)$$

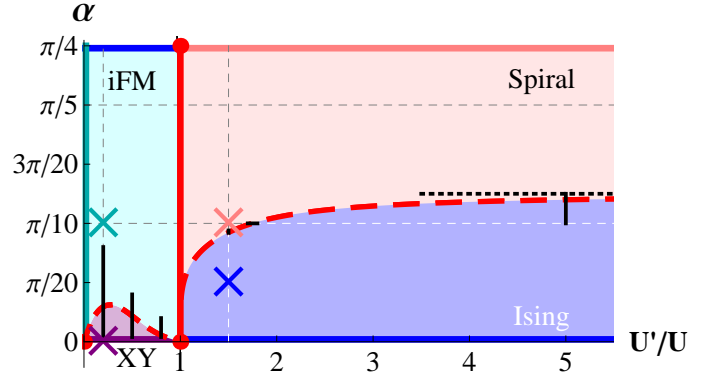


Figure 2: (Color online) Phase diagram of Hamiltonian (7) as a function of parameters U'/U and α obtained by DMRG calculations of the ground state. We distinguish two gapped phases: an *Ising* phase (dark blue) and one with incomplete ferromagnetic order (*iFM*) (light blue); and two gapless phases: an *XY* phase (purple) and a *spiral* phase (pink). The plain lines indicate when the model maps onto a XXZ model, in which case the phase is known a priori. The colored crosses locate the points which are analyzed in Figs. 3 and 6, and the dotted gray lines locate the cuts analyzed in Figs. 4, 5 and 7. The dashed black line indicate the transition point in the $U'/U \rightarrow \infty$ limit, known analytically. The red lines indicate critical lines: the dashed red lines are estimations of the phase boundary obtained by DMRG calculations (error bars are displayed in black) and the boundary at $U'/U = 1$ is known a priori (see text).

The phase diagram of this model is presented in Fig. 2 and will be explained in detail in the remainder of the paper. We only consider the region $0 < \alpha < \pi/4$, since the rest can be deduced by simple transformations. Indeed, Eq. (7) is π -periodic in α , and if $\pi/4 < \alpha < \pi/2$, by setting $\alpha' = \pi/2 - \alpha$, $S_j^x = (-1)^j S_j'^x$, $S_j^y = S_j'^y$ and $S_j^z = (-1)^j S_j'^z$, we recover Hamiltonian (7) with $0 < \alpha' < \pi/4$. In some particular cases (signaled by plain lines in Fig. 2), Eq. (7) can be mapped onto a XXZ model, in which case the phases are known ab-initio, as in Sec. III. However, for general values of U'/U and α , the DM term cannot be gauged away, and this model can hardly be handled analytically. We therefore explore the phase diagram numerically by computing the ground state of Hamiltonian (7) by the Density Matrix Renormalization Group (DMRG) method [42, 43]. In the calculations we use a finite-size DMRG algorithm, for systems of total sizes up to $L = 500$ lattice sites with open boundary conditions. We keep up to $m = 1000$ states in the matrix product state representation. Once the calculations are converged, the truncation error of the reduced density matrix is typically 10^{-8} and the energies are converged up to the 10^{th} digit.

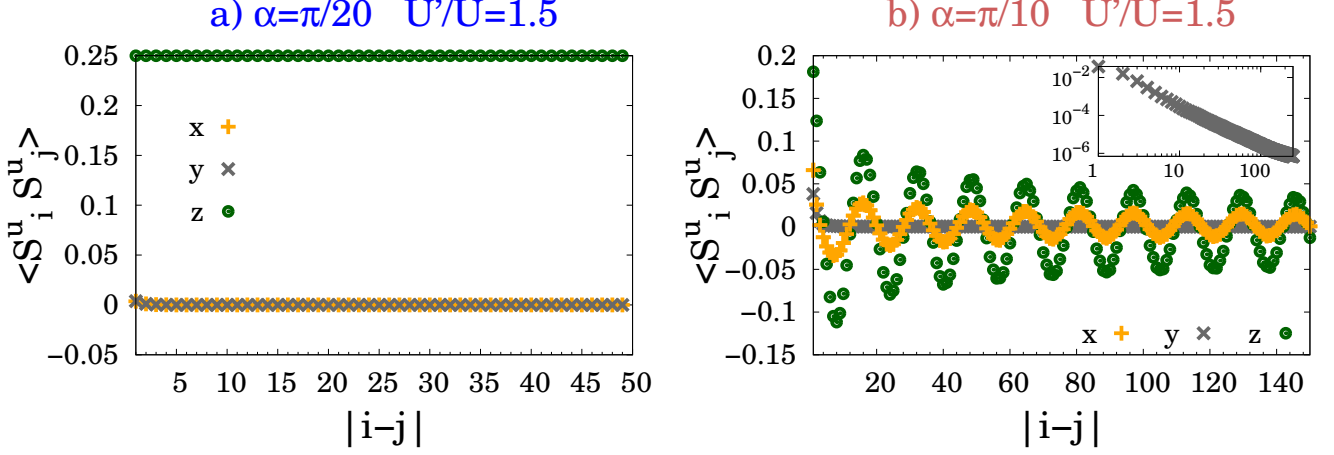


Figure 3: (Color online) Correlation functions in the ground state of Hamiltonian (7) obtained by DMRG calculations. Shown are $\langle S_i^x S_j^x \rangle$ (orange plus signs), $\langle S_i^y S_j^y \rangle$ (gray crosses) and $\langle S_i^z S_j^z \rangle$ (green dots) for (a) $\alpha = \pi/20$ and $U'/U = 1.5$ and (b) $\alpha = \pi/10$ and $U'/U = 1.5$. The inset of (b) show $\langle S_i^y S_j^y \rangle$ in log/log scale. For the sake of clarity those points are identified in Fig. 2 by crosses.

A. $U' > U$ – Ising to spiral phase transition

Let us first analyze the region $U' > U$ of the phase diagram, where two different phases exist. The spin-spin correlation functions $\langle S_i^u S_j^u \rangle$ (with $u \in \{x, y, z\}$) of these two phases in the ground state are presented in figure 3. To get some insight, we first focus on several special points (lines) in the phase diagram.

Firstly, along the $\alpha = 0$ axis, Eq. (7) becomes a XXZ model:

$$\mathcal{H}_s^{\alpha=0} = J_0 \sum_j \left[- (S_j^x S_{j+1}^x + S_j^y S_{j+1}^y) + \left(-2 \frac{U'}{U} + 1 \right) S_j^z S_{j+1}^z \right]. \quad (8)$$

For $U'/U > 1$ the ground state is therefore an Ising state with perfect FM ordering along the z -direction [46]. For small values of α , the term $-S_j^z S_{j+1}^z$ still dominates in \mathcal{H}_s and it is easy to prove that the ground state is still a nearly-perfect FM phase (a gapped Ising-type phase) as shown in the dark blue region in phase diagram of Fig. 2. This can be numerically verified by the spin-spin correlation functions as shown in Fig. 3(a), where we can observe that in this regime the ground state exhibits nearly-perfect FM order in the z -direction with $\langle S_i^z S_j^z \rangle \simeq 1/4$ for any $|i-j|$.

Secondly, if we focus on the line $\alpha = \pi/4$, the Hamiltonian of Eq. (7) is given by

$$\mathcal{H}_s^{\alpha=\pi/4} = J_0 \sum_j \left[-S_j^y S_{j+1}^y + \frac{U'}{U} (S_j^z S_{j+1}^x - S_j^x S_{j+1}^z) \right]. \quad (9)$$

After a rotation of the local basis of each spin \mathbf{S}_i by an angle $j\pi/2$ around axis y this maps onto $\mathcal{H}_s^{\alpha=\pi/4} =$

$J_0 \sum_j -S_j'^y S_{j+1}'^y + \frac{U'}{U} (S_j'^x S_{j+1}'^x + S_j'^z S_{j+1}'^z)$. Therefore, for $U'/U > 1$, the system is in a gapless ‘XY phase’ [46] (with uniaxial symmetry around the y -axis). It features algebraic decay of the correlations, and a spiral order with a 4-site period along y , due to the rotation of the mapping. This picture does not qualitatively change when α is close to $\pi/4$, in which case the DM term dominates in Eq. (7), and we find a spiral phase around the y -direction in the region of Fig. 2 shaded in pink. The correlations also decay algebraically [see Fig. 3(b)], signaling a gapless Luttinger-liquid phase [49]. Moreover, we find that the correlations $\langle S_i^u S_j^u \rangle$ in the x and z -directions oscillate with the same period, thus showing spiral order [50]. Note that the spiral does not have the same amplitude in the x and z -directions, due to the anisotropy in the exchange term in Eq. (7).

In the limit $U'/U \rightarrow \infty$, the Hamiltonian in Eq. (7) reduces to

$$\mathcal{H}_s^{\frac{U'}{U} \rightarrow \infty} \simeq J_0 \frac{U'}{U} \sum_j \left[-2 \cos(2\alpha) S_j^z S_{j+1}^z + \sin(2\alpha) (S_j^z S_{j+1}^x - S_j^x S_{j+1}^z) \right], \quad (10)$$

which can be solved exactly by performing a rotation in spin space followed by the Jordan-Wigner transformation [49, 52]. Equation (10) can be mapped to a noninteracting spinless fermion Hamiltonian, with the dispersion relation:

$$\epsilon_k^\pm = J_0 \frac{U'}{U} \left[\frac{\tan(2\alpha)}{2} \sin(k) \pm \frac{1}{2} \right], \quad (11)$$

where k is the wavevector in units of the reciprocal lattice spacing. One immediately finds a phase transition from a gapped phase to a gapless phase with increasing α , with

the phase transition taking place at $\alpha_c = \pi/8$. This value is represented as a dotted black line in Fig. 2.

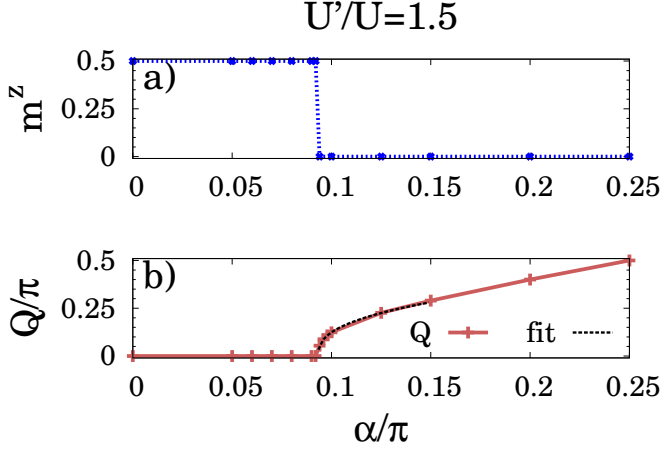


Figure 4: (Color online) (a) Magnetization m^z in the z -direction and (b) ordering wavevector Q at constant $U'/U = 1.5$. This cut is highlighted in Fig. 2 by a dashed gray line. The magnetization is extracted from correlation functions in the ground state with $m^z = \sqrt{\lim_{|i-j| \rightarrow \infty} \langle S_i^z S_j^z \rangle}$ and Q from large-distance fits of $\langle S_i^x S_j^x \rangle$ and $\langle S_i^z S_j^z \rangle$ by $\cos(Q|i-j|)/|i-j|^\gamma$ with Q and γ as fitting parameters. In (b) the data near the transition point is fitted by $Q \propto (\alpha - \alpha_c)^\delta$ with δ a fitting parameter (black dashed line). The fit gives $\alpha_c = 0.093\pi$ and $\delta = 0.38$.

For finite values of U'/U , the problem can no longer be solved analytically. We have thus computed the ground state properties with DMRG. The magnetization $m^z = \sqrt{\lim_{|i-j| \rightarrow \infty} \langle S_i^z S_j^z \rangle}$ is plotted in Fig. 4(a) as a function of α for fixed $U'/U = 1.5$. This shows that for small α the ground state is a nearly-perfect ferromagnet. At the transition point [$\alpha_c \simeq (0.093 \pm 0.001)\pi$], the magnetization suddenly drops to 0, therefore signaling a first-order phase transition.

Another way to characterize the phase transition is to compute the characteristic wavevector Q of the spiral phase, in which the correlations become incommensurate. The incommensurability leads to a shift of the peak in the structure factor $S_a(q) = \langle \sum_{i,j} e^{iq(i-j)} S_i^u S_j^u \rangle / L$, with L the system size, from the position $q = 0$ to $q = \pm Q$, where the peaks are broadened by the decay of correlations and possibly finite-size effects. We obtain the characteristic wavevector Q by fitting $\langle S_i^x S_j^x \rangle$ and $\langle S_i^z S_j^z \rangle$ by $\cos(Q|i-j|)/|i-j|^\gamma$ with Q and γ as fitting parameters. The characteristic wavevector Q as a function of α is shown in Fig. 4(b). We find that Q increases continuously from zero when crossing the critical point. At the transition, it exhibits a singularity compatible with $Q(\alpha) \propto (\alpha - \alpha_c)^\delta$ as can be seen from the fit in Fig. 4(b). At $\alpha = \pi/4$, Q reaches $\pi/2$, which agrees with our previous analysis [see Eq. (9) and below].

The critical value α_c obtained above for $U'/U = 1.5$

is marked in Fig. 2, together with an estimation of the transition point along the lines $U'/U = 5$ and $\alpha = \pi/10$ [see also Fig. 5(b) below]. The critical line for this transition must eventually bend down to reach the point $(\alpha, U'/U) = (0, 1)$, because the line $U'/U = 1$ is a spiral critical phase (see below); hence the phase diagram for $U'/U > 1$ as shown in Fig. 2.

B. $U' \simeq U$ – Incomplete ferromagnet to spiral phase transition

Now, we focus on the regime $U' \simeq U$. We again start by analyzing the special cases of the phase diagram to get some intuition.

In the case $U' = U$, Hamiltonian (7) reads

$$\mathcal{H}_s^{U'/U=1} = J_0 \sum_j \left[-\cos(2\alpha) (S_j^x S_{j+1}^x + S_j^z S_{j+1}^z) - S_j^y S_{j+1}^y + \sin(2\alpha) (S_j^z S_{j+1}^x - S_j^x S_{j+1}^z) \right], \quad (12)$$

and a rotation of the local basis of each spin \mathbf{S}_i by an angle $2j\alpha$ around axis y allows us to gauge out the DM term [24]. The model then reduces to an isotropic FM Heisenberg model $\mathcal{H}_s^{U'/U=1} = -\mathbf{S}_j \cdot \mathbf{S}_{j+1}$. In that case, the ground state is a gapless FM state with high degeneracy, which is also the critical state in the XXZ model [46].

Figure 5 displays $m^y = \sqrt{\lim_{|i-j| \rightarrow \infty} \langle S_i^y S_j^y \rangle}$, m^z and the characteristic wavevector Q in the spiral phase as a function of U'/U with fixed $\alpha = \pi/5$ [Fig. 5 (a)] and $\pi/10$ [Fig. 5 (b)] respectively. In both cases we find that $U'/U = 1$ is indeed the critical point of a first-order transition between a gapless spiral phase and a gapped phase with long-range FM order along the y -direction ($m^y \neq 0$). We name this phase ‘incomplete ferromagnet’ (iFM) in the following, since $m^y < 1/4$. It is found in the top-left corner of the phase diagram (blue-shaded region in Fig. 2), a region in which the Hamiltonian is dominated by $-S_j^y S_{j+1}^y$. Figure 6(a) shows the spin-spin correlation functions at $U'/U = 0.2$ and $\alpha = \pi/10$. We indeed find a reduced magnetization in the y -direction: $\lim_{|i-j| \rightarrow \infty} \langle S_i^y S_j^y \rangle \simeq 0.062 < 1/4$. We also observe that the correlations along the x and z -directions decay exponentially, indicating a gapped phase. The nature of the iFM state can be understood in the limit $U'/U = 0$, where Eq. (7) becomes

$$\mathcal{H}_s^{U'/U=0} = J_0 \sum_j \left[\cos(2\alpha) (-S_j^x S_{j+1}^x + S_j^z S_{j+1}^z) - S_j^y S_{j+1}^y \right]. \quad (13)$$

After the rotation of each spin \mathbf{S}_j around the z -axis by an angle $j\pi$ [$S_j^x = (-1)^j S_{j+1}^x$, $S_j^y = (-1)^j S_{j+1}^y$ and $S_j^z = S_{j+1}^z$], the model maps to an antiferromagnetic (AF) XXZ model in the Néel phase (with preferred axis y). Unlike for the FM XXZ model, it is known that the perfect

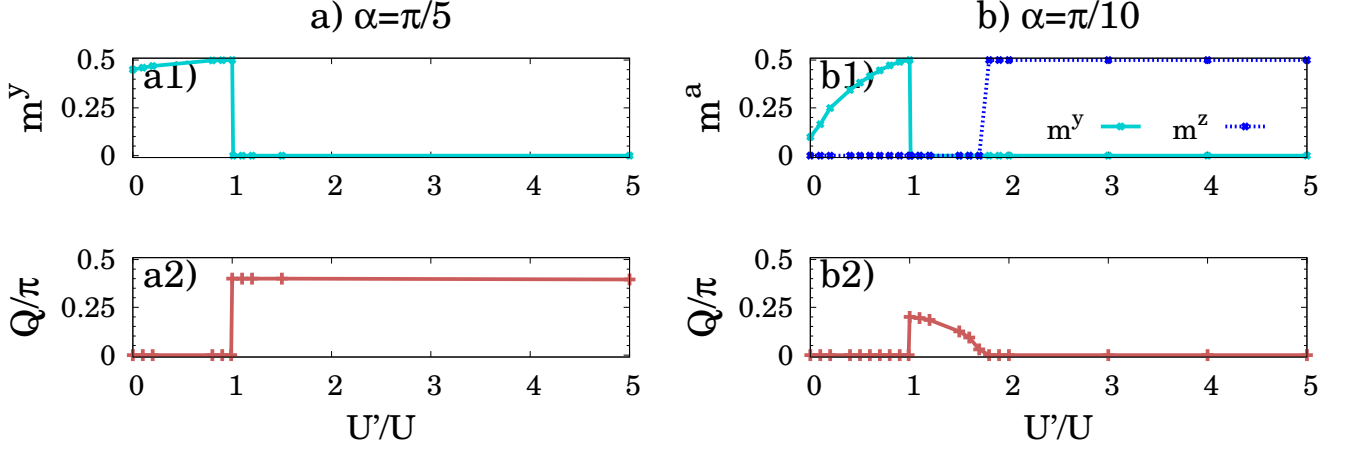


Figure 5: (Color online) Magnetization $m^{y,z}$ in the y and z -directions and ordering wavevector Q along two cuts in the phase diagram: (a) constant $\alpha = \pi/5$ and (b) constant $\alpha = \pi/10$. Those cuts are highlighted in Fig. 2 by dashed gray lines. The magnetization is extracted from correlation functions in the ground state with $m^{y,z} = \sqrt{\lim_{|i-j| \rightarrow \infty} \langle S_i^{y,z} S_j^{y,z} \rangle}$ and Q from large-distance fits of $\langle S_i^x S_j^x \rangle$ and $\langle S_i^z S_j^z \rangle$ by $\cos(Q|i-j|)/|i-j|^\gamma$.

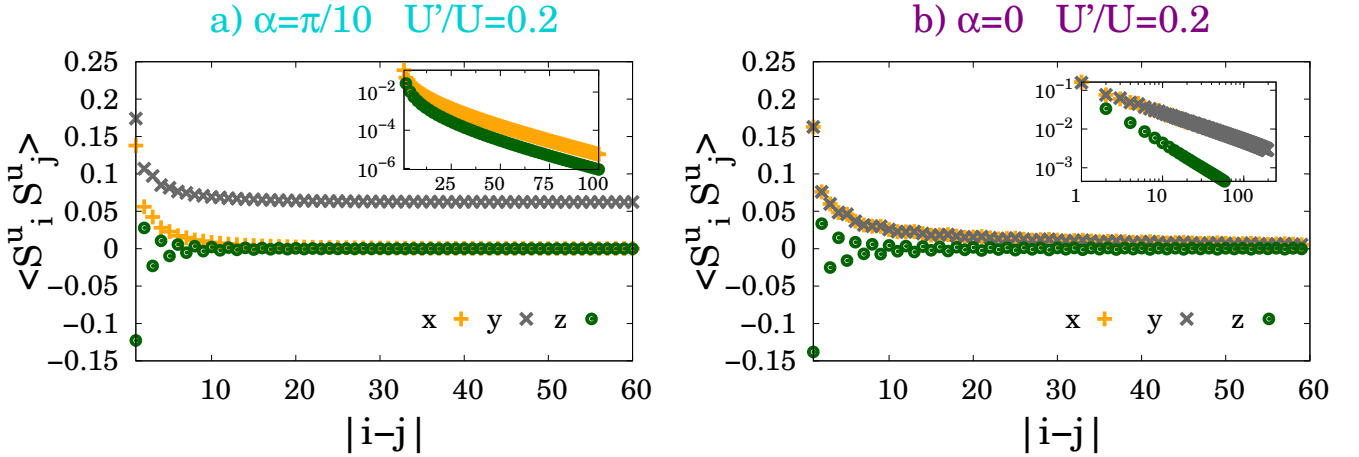


Figure 6: (Color online) Correlation functions in the ground state of Hamiltonian (7) obtained by DMRG calculations. Shown are $\langle S_i^x S_j^x \rangle$ (orange plus signs), $\langle S_i^y S_j^y \rangle$ (gray crosses) and $\langle S_i^z S_j^z \rangle$ (green dots) for (a) $\alpha = \pi/10$ and $U'/U = 0.2$ and (b) $\alpha = 0$ and $U'/U = 0.2$. The insets show the same data in log/linear scale for (a), and in log/log scale for (b). For the sake of clarity those points are identified in Fig. 2 by crosses.

AF state along the y -axis (which would correspond to a perfect FM state along the y -direction after the above rotation) is not the ground state of the AF XXZ model in the Néel phase. Therefore, after the above spin rotation, the ground state of Eq. (13) exhibits FM order with reduced magnetization along the y -axis.

We therefore find that the transition from the iFM phase to the incommensurate spiral phase is again a first-order phase transition. As can be seen in Figs. 5(a2) and (b2), the onset of incommensurability also coincides with the transition point. However, unlike the Ising to spiral phase transition analyzed previously (see Sec. IV A), we find that the characteristic wavevector jumps discontinu-

ously from 0 (in the commensurate iFM phase) to a finite value $Q = 2\alpha$. In Fig. 5(a2) we observe that the value of Q is rather constant in the spiral phase, along a cut at $\alpha = \pi/5$. In the cut at $\alpha = \pi/10$ [Fig. 5(b2)] however, Q decreases and reaches 0 at $U'/U \simeq 1.75 \pm 0.01$, at the point where the magnetization m^z jumps to 0.5, indicating a transition to the Ising phase (nearly-perfect FM phase).

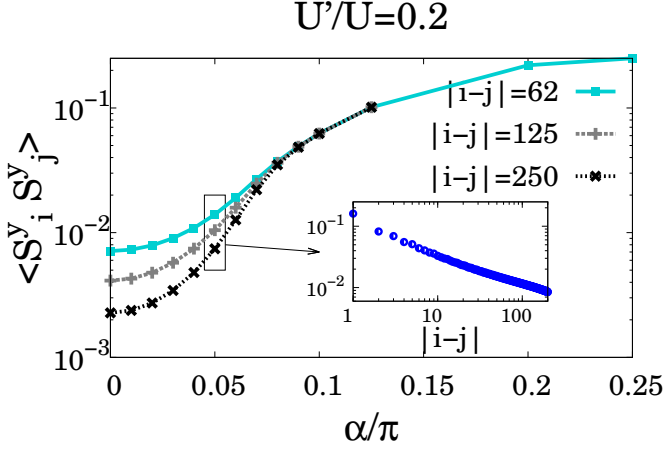


Figure 7: (Color online) Spin-spin correlations $\langle S_i^y S_j^y \rangle$, at constant $U'/U = 0.2$, in logarithmic scale. They are computed in the ground state obtained by DMRG, around the center of a system of total size $L = 500$, for different site distances: $|i - j| = 50$ (plain blue line), 125 (dashed grey line) and 250 (dotted black line). This cut is highlighted in Fig. 2 by a dashed gray line. The inset shows the full function $\langle S_i^y S_j^y \rangle$ for $\alpha = \pi/20$, in log/log scale.

C. $U' < U$ – Incomplete ferromagnet to XY phase transition

Finally, we study the quantum phases and transitions in the region $U' < U$, and again first focus on some special points or lines in the phase diagram to get some insight.

We note firstly that in the limit $\alpha = 0$ [see Eq. (8)], the ground state for $0 < U'/U < 1$ is a gapless XY phase [46]. In this phase, all correlation functions decay algebraically, as shown in Fig. 6(b) for $U'/U = 0.2$ and $\alpha = 0$. We expect that a small α will not qualitatively change the nature of this gapless phase. Therefore, there should be a phase transition to the gapped iFM phase with increasing α . Such a gapless phase with respect to spin excitations is also predicted in Ref. [30].

Let us focus on this phase transition. Along the $U'/U = 0$ line, as we have analyzed above, the Hamiltonian maps onto an AF XXZ model [see Eq. (13) and below], and the ground state is always of gapped iFM type for all $\alpha > 0$, while the point at $(\alpha, U'/U) = (0, 0)$ is a critical point of Berezinskii-Kosterlitz-Thouless (BKT) type [46, 47]. Therefore, for small α , the excitation gap is exponentially small, and varies as $\Delta \sim e^{-\pi/(\sqrt{2}\alpha)}$ [46, 47], which makes it very difficult to numerically distinguish the gapless from the gapped phase.

In figure 7, we show the correlation $\langle S_i^y S_j^y \rangle$ as a function of α for $U'/U = 0.2$ and various site separations $|i - j|$. For large α (e.g. $\alpha > \pi/10$), spin-spin correlations along the y -direction saturate to a non-zero value

at large distances, which indicates the existence of FM long range ordering, while for smaller α (e.g. $\alpha = \pi/20$), the spin-spin correlations decay algebraically at large distances (as shown in the inset of Fig. 7), which seems to indicate a gapless phase. However, due to the numerical precision and limitations in the system size of our numerical calculations, we cannot exclude the possibility that it is a gapped phase with an extremely small gap, just as the situation near the BKT phase transition. In which case the spin correlations would saturate to an extremely small value. It is therefore difficult to locate the position of the assumed transition point precisely. However, our data clearly provide an upper bound for the phase transition point. Indeed, the ground state at $\alpha = \pi/10$ has finite magnetization, and the other correlation functions $\langle S_i^x S_j^x \rangle$ and $\langle S_i^z S_j^z \rangle$ decrease exponentially with $|i - j|$ [see Fig. 6(a)]. We confirmed using infinite-size DMRG that the correlation length saturates in the thermodynamic limit to a finite value [we find $\xi = 21.16$ lattice sites for the parameters of Fig. 6(a)], thus demonstrating unambiguously that this point is in the gapped iFM phase. Our numerical result indicates that there is a continuous phase transition between the iFM and the XY phase (the purple regime in Fig. 2). However, as we analyzed before, we cannot preclude here the possibility that there is no phase transition at finite α , and that the gapless regime shrinks to a critical line with $\alpha = 0$.

V. CONCLUSION AND DISCUSSION

In this paper we have studied the quantum magnetism of the Mott insulating phases found in the strongly interacting limit of the 1D Bose-Hubbard model with both abelian and non-abelian synthetic gauge fields. In the abelian case (spin-dependent magnetic field) which is relevant to current experiments with cold atoms, we found that the ground state exhibits a spiral quasi long-range order in the regime $U'/U < 1$. In the non-abelian case (Rashba spin-orbit coupling), we have studied the phase diagram of the effective Hamiltonian, where we identified four phases with different magnetic textures: two gapped phases with nearly-complete (Ising) and incomplete (iFM) ferromagnetic order and two gapless phases with and without spiral quasi long-range order. We have found that the transitions between the ferromagnetic phases and the spiral phase are both first order, and the emergence of the incommensurability in the spiral phase coincides with the phase transition. The ordering wavevector is continuous at the Ising to spiral phase transition, whereas it is discontinuous at the iFM to spiral one. Finally, in the regime $U'/U < 1$, there is a continuous phase transition from an XY phase to a gapped iFM phase, for small α .

We have focused here on situations in which only one component of the DM interaction is non-zero. However, the general model given in Eq. (4) allows more than one component for the DM vector \mathbf{D} , in the case where both

the abelian and the non-abelian synthetic gauge fields are present. This may give rise to richer quantum magnetic phases and deserves to be explored in the future. We have also focused on the 1D case. However, DM interactions are also very interesting in 2D, as they can give rise to exotic topological magnetic textures such as vortex and skyrmion crystals: topics that could also be addressed with ultracold atoms [24–26].

Note – During the completion of this manuscript, we became aware of the work reported in Refs. [53–55], which address a similar topic.

VI. ACKNOWLEDGMENTS

We thank Fabian Heidrich-Meisner, Vincenzo Alba and Lode Pollet for enlightening discussions. This research was supported by DFG FOR 801. This work was partly supported by the Australian Research Council grant CE110001013.

-
- [1] D. Jaksch and P. Zoller, *New J. Phys.* **5**, 56 (2003).
 - [2] J. Dalibard, F. Gerbier, G. Juzeliūnas, and P. Öhberg, *Rev. Mod. Phys.* **83**, 1523 (2011).
 - [3] V. Galitski and I. B. Spielman, *Nature (London)* **494**, 49 (2013).
 - [4] Y.-J. Lin, R. L. Compton, K. Jiménez-García, J. V. Porto, and I. B. Spielman, *Spin-orbit-coupled bose-einstein condensates* (2009).
 - [5] M. Aidelsburger, M. Atala, S. Nascimbène, S. Trotzky, Y.-A. Chen, and I. Bloch, *Phys. Rev. Lett.* **107**, 255301 (2011).
 - [6] Y.-J. Lin, K. Jiménez-García, and I. B. Spielman, *Nature (London)* **471**, 83 (2011).
 - [7] D. R. Hofstadter, *Phys. Rev. B* **14**, 2239 (1976).
 - [8] M. Aidelsburger, M. Atala, M. Lohse, J. T. Barreiro, B. Paredes, and I. Bloch, *Phys. Rev. Lett.* **111**, 185301 (2013).
 - [9] H. Miyake, G. A. Siviloglou, C. J. Kennedy, W. C. Burton, and W. Ketterle, *Phys. Rev. Lett.* **111**, 185302 (2013).
 - [10] C. Wu, I. Mondragon-Shem, and X.-F. Zhou, *Chinese Phys. Lett.* **28**, 097102 (2008).
 - [11] T. D. Stanescu, B. Anderson, and V. Galitski, *Phys. Rev. A* **78**, 023616 (2008).
 - [12] C. Wang, C. Gao, C.-M. Jian, and H. Zhai, *Phys. Rev. Lett.* **105**, 160403 (2010).
 - [13] T. Graß, K. Saha, K. Sengupta, and M. Lewenstein, *Phys. Rev. A* **84**, 053632 (2011).
 - [14] T.-L. Ho and S. Zhang, *Phys. Rev. Lett.* **107**, 150403 (2011).
 - [15] H. Hu, B. Ramachandhran, H. Pu, and X.-J. Liu, *Phys. Rev. Lett.* **108**, 010402 (2012).
 - [16] Y. Zhang, L. Mao, and C. Zhang, *Phys. Rev. Lett.* **108**, 035302 (2012).
 - [17] X. Zhou, Z. Cai, and C. Wu, *J. Phys. B: At. Mol. Opt. Phys.* **46**, 134001 (2013).
 - [18] P. Wang, Z.-Q. Yu, Z. Fu, J. Miao, L. Huang, S. Chai, H. Zhai, and J. Zhang, *Phys. Rev. Lett.* **109**, 095301 (2012).
 - [19] L. W. Cheuk, A. T. Sommer, Z. Hadzibabic, T. Yefsah, W. S. Bakr, and M. W. Zwierlein, *Phys. Rev. Lett.* **109**, 095302 (2012).
 - [20] C. J. Kennedy, G. A. Siviloglou, H. Miyake, W. C. Burton, and W. Ketterle, *Phys. Rev. Lett.* **111**, 225301 (2013).
 - [21] D. Pesin and L. Balents, *Nature Phys.* **6**, 376 (2010).
 - [22] S. Rachel and K. Le Hur, *Phys. Rev. B* **82**, 075106 (2010).
 - [23] D. Cocks, P. P. Orth, S. Rachel, M. Buchhold, K. Le Hur, and W. Hofstetter, *Phys. Rev. Lett.* **109**, 205303 (2012).
 - [24] Z. Cai, X. Zhou, and C. Wu, *Phys. Rev. A* **85**, 061605 (2012).
 - [25] J. Radić, A. Di Ciolo, K. Sun, and V. Galitski, *Phys. Rev. Lett.* **109**, 085303 (2012).
 - [26] W. S. Cole, S. Zhang, A. Paramekanti, and N. Trivedi, *Phys. Rev. Lett.* **109**, 085302 (2012).
 - [27] S. Mandal, K. Saha, and K. Sengupta, *Phys. Rev. B* **86**, 155101 (2012).
 - [28] M. Gong, Y. Qian, V. W. Scarola, and C. Zhang (2013), arXiv:1205.6211.
 - [29] P. P. Orth, D. Cocks, S. Rachel, M. Buchhold, K. Le Hur, and W. Hofstetter, *J. Phys. B: At. Mol. Opt. Phys.* **46**, 134004 (2013).
 - [30] J. Zhao, S. Hu, J. Chang, P. Zhang, and X. Wang, *Phys. Rev. A* **89**, 043611 (2014).
 - [31] L.-M. Duan, E. Demler, and M. D. Lukin, *Phys. Rev. Lett.* **91**, 090402 (2003).
 - [32] A. B. Kuklov and B. V. Svistunov, *Phys. Rev. Lett.* **90**, 100401 (2003).
 - [33] I. E. Dzyaloshinsky, *J. Phys. Chem. Sol.* **4**, 241 (1958).
 - [34] T. Moriya, *Phys. Rev.* **120**, 91 (1960).
 - [35] D. Coffey, T. M. Rice, and F. C. Zhang, *Phys. Rev. B* **44**, 10112 (1991).
 - [36] N. E. Bonesteel, *Phys. Rev. B* **47**, 11302 (1993).
 - [37] M. Oshikawa and I. Affleck, *Phys. Rev. Lett.* **79**, 2883 (1997).
 - [38] I. Affleck and M. Oshikawa, *Phys. Rev. B* **60**, 1038 (1999).
 - [39] L. Shekhtman, O. Entin-Wohlman, and A. Aharony, *Phys. Rev. Lett.* **69**, 836 (1992).
 - [40] S. Inouye, M. R. Andrews, J. Stenger, H.-J. Miesner, D. M. Stamper-Kurn, and W. Ketterle, *Nature (London)* **392**, 151 (1998).
 - [41] E. A. Donley, N. R. Claussen, S. Thompson, and C. E. Wieman, *Nature (London)* **417**, 529 (2002).
 - [42] S. R. White, *Phys. Rev. Lett.* **69**, 2863 (1992).
 - [43] U. Schollwöck, *Rev. Mod. Phys.* **77**, 259 (2005).
 - [44] M. Atala, M. Aidelsburger, M. Lohse, J. T. Barreiro, B. Paredes, and I. Bloch (2014), arXiv:1402.0819.
 - [45] M. Brockmann, A. Klümper, and V. Ohanyan, *Phys. Rev. B* **87**, 054407 (2013).
 - [46] U. Schollwöck, J. Richter, D. J. Farnell, and R. F. Bishop (Eds.) (Springer, Berlin Heidelberg, 2004).
 - [47] S. Sachdev (Cambridge University Press, 2011).
 - [48] K. Osterloh, M. Baig, L. Santos, P. Zoller, and M. Lewenstein

- stein, Phys. Rev. Lett. **95**, 010403 (2005).
- [49] M. A. Cazalilla, R. Citro, T. Giamarchi, E. Orignac, and M. Rigol, Rev. Mod. Phys. **83**, 1405 (2011).
 - [50] In cold-atom setups, S_j^z is given by the population imbalance ($S_j^z = n_{j,\uparrow} - n_{j,\downarrow}$) and spin-spin correlations are accessible [51].
 - [51] J. Imriška, M. Iazzi, L. Wang, E. Gull, D. Greif, T. Uehlinger, G. Jotzu, L. Tarruell, T. Esslinger, and M. Troyer, Phys. Rev. Lett. **112**, 115301 (2014).
 - [52] P. Jordan and E. Wigner, Z. Phys. **47**, 631 (1928).
 - [53] J. Zhao, S. Hu, J. Chang, F. Zheng, P. Zhang, and X. Wang (2014), arXiv:1403.1316.
 - [54] Z. Xu, W. Cole, and S. Zhang, Phys. Rev. A **89**, 051604 (2014).
 - [55] S. Peotta, L. Mazza, E. Vicari, M. Polini, R. Fazio, and D. Rossini (2014), arXiv:1403.4568.